International Journal of Thermal Sciences 48 (2009) 1627–1638

Contents lists available at ScienceDirect

International Journal of Thermal Sciences

www.elsevier.com/locate/ijts

Numerical study of the inlet/outlet arrangement effect on microchannel heat sink performance

Reiyu Chein *, Janghwa Chen

Department of Mechanical Engineering, National Chung Hsing University, 250 Kuo-Kuang Rd., Taichung City, Taiwan 402

ARTICLE INFO

Article history:
Received 7 August 2008
Received in revised form 2 November 2008
Accepted 23 December 2008
Available online 20 January 2009

Keywords:
Microchannel heat sink
Inlet/outlet arrangements
Velocity and temperature maldistribution
Thermal resistance
Pressure drop coefficient

ABSTRACT

In this study, fluid flow and heat transfer in microchannel heat sinks are numerically investigated. The three-dimensional governing equations for both fluid flow and heat transfer are solved using the finite-volume scheme. The computational domain is taken as the entire heat sink including the inlet/outlet ports, inlet/outlet plenums, and microchannels. The particular focus of this study is the inlet/outlet arrangement effects on the fluid flow and heat transfer inside the heat sinks.

The microchannel heat sinks with various inlet/outlet arrangements are investigated in this study. All of the geometric dimensions of these heat sinks are the same except the inlet/outlet locations. Because of the difference in inlet/outlet arrangements, the resultant flow fields and temperature distributions inside these heat sinks are also different under a given pressure drop across the heat sink. Using the averaged velocities and fluid temperatures in each channel to quantify the fluid flow and temperature maldistributions, it is found that better uniformities in velocity and temperature can be found in the heat sinks having coolant supply and collection vertically via inlet/outlet ports opened on the heat sink cover plate. Using the thermal resistance, overall heat transfer coefficient and pressure drop coefficient to quantify the heat sink performance, it is also found these heat sinks have better performance among the heat sinks studied. Based on the results from this study, it is suggested that better heat sink performance can be achieved when the coolant is supplied and collected vertically.

1. Introduction

With the advancements in computing technology in the past few decades, electronics have become faster, smaller and more powerful. This results in an ever-increasing heat generation rate from electronic devices. In most cases, the chips are cooled through forced air flow. However, when dealing with components that contain billions of transistors working at high frequency, the temperature can reach a critical level where standard cooling methods are not sufficient. In addition to high-performance electronic chips, high heat flux removal is also required in devices such as laser diode arrays and high-energy mirrors. In the past two decades, many cooling technologies have been pursued to meet the requirements of high heat dissipation rate and maintaining a low junction temperature. Among these efforts, the microchannel heat sink has received much attention because of its ability to produce high heat transfer coefficient, its' small size and volume per heat load, and small coolant requirements. Recent progress in the development of microchannel heat sinks is provided by Kandlikar and Grande [1].

A microchannel heat sink typically contains a large number of parallel microchannels with a hydraulic diameter ranging from 10 to 1000 μm. Coolant is forced to pass through these channels to carry the heat away from a hot surface. The heat sink cooling concept was first proposed for electronic cooling by Tuckerman and Pease [2]. Since then, microchannel heat sink performance using different substrate materials and channel dimensions have been studied extensively in the past two decades. These studies can be categorized into theoretical [3–6], numerical [7–11], and experimental approaches [12–16]. In the theoretical approach, the main objective is to develop design schemes that can be used to optimize microchannel heat sink performance. Most studies in this approach employed the classical fin theory which models the solid walls separating microchannels as the thin fins. The heat transfer process is simplified as one-dimensional, constant convection heat transfer coefficient and uniform fluid temperature. However, the nature of the heat transfer process in a microchannel heat sink is conjugated heat conduction in the solid wall and convection to the cooling fluid. The simplifications used in the theoretical approach usually under- or over predict the microchannel heat sink performance.

Although experimental studies have been carried out extensively in the past, it is often difficult to employ conventional measurement techniques with microchannel heat sinks to extract data

* Corresponding author.
E-mail address: rychein@dragon.nchu.edu.tw (R. Chein).

1290-0729/$ – see front matter
doi:10.1016/j.ijthermalsci.2008.12.019

Nomenclature

c_p	specific heat	$J\,kg^{-1}\,K^{-1}$	
D_h	hydraulic diameter of the channel	m	
H_{ch}	depth of the microchannel	m	
F	heat sink pressure drop coefficient	m^{-4}	
$\bar{h}$	overall heat transfer coefficient of heat sink	$W\,m^{-2}\,K^{-1}$	
H_{hs}	depth of heat sink	m	
H_{ch}	depth of microchannel	m	
k	fluid thermal conductivity	$W\,m^{-1}\,K^{-1}$	
k_s	solid fluid thermal conductivity	$W\,m^{-1}\,K^{-1}$	
L_{ch}	length of microchannel	m	
L_{hs}	length of heat sink	m	
$\dot{m}$	mass flow rate	$kg\,sec^{-1}$	
$\overline{Nu}$	overall Nusselt number of heat sink		
p	pressure	kPa	
$\Delta p_{in,1}$	pressure drop from inlet port to inlet plenum	kPa	
$\Delta p_{in,2}$	pressure drop at the channel inlet	kPa	
Δp_{ch}	pressure drop across the channel	kPa	
$\Delta p_{ex,1}$	pressure drop from channel exit to the outlet plenum	kPa	
$\Delta p_{ex,2}$	pressure drop from the outlet plenum to the outlet port	kPa	
Pr	fluid Prandtl number		
Q	fluid flow rate	$m^3\,sec^{-1}$	
Q_{flow}	heat absorbed by fluid	W	
q_w	heat flux at microchannel heat sink base plate	$W\,m^{-2}$	
R_{th}	heat sink thermal resistance	$K\,W^{-1}$	
Re_{D_h}	Reynolds number based on hydraulic diameter		
$x_{fd,t}$	thermal entrance length	m	
T	fluid phase temperature	K	
$T_{hs,ave}$	averaged temperature of the entire heat sink solid part	K	
T_{ave}	averaged fluid temperature in the heat sink	K	
T_b	fluid bulk temperature	K	
T_s	microchannel heat sink solid temperature	K	
T_{in}	fluid inlet temperature	K	
$\bar{T}_w$	local averaged microchannel wall temperature	K	
$\vec{V}$	fluid velocity	$m\,sec^{-1}$	
T_{out}	fluid outlet temperature	K	
$\dot{V}$	coolant volumetric flow rate	mL/min	
W_{ch}	width of microchannel	m	
W_{fin}	width of microchannel wall	m	
W_{hs}	width of the heat sink	m	

Greek symbols

μ	viscosity	$kg\,m^{-1}\,sec^{-1}$
ρ	density	$kg\,m^{-3}$

that are important to characterizing the fluid flow and heat transfer such as local fluid and wall temperature distributions. For this reason, numerical simulation becomes a necessary tool that offers more quantitative insight into the transport process in the microchannel heat sink. In the numerical simulation, conventional equations governing the fluid flow and heat transfer are assumed to be still valid in the micro-scale dimension. The conjugate heat transfer process between the fluid and solid wall is included. Fedorov and Viskanta [7] numerically analyzed three-dimensional conjugate heat transfer in a microchannel heat sink without the hydrodynamic and thermal fully developed flow assumptions. They obtained very complicated heat transfer pattern characterized by a nearly uniform microchannel wall temperature and the negative local heat transfer at the channel corners. Ambatipudi and Rahman [8] performed numerical simulations for conjugate heat transfer in microchannel heat sink by varying the channel depth, channel width, number of channel, and flow rate. They found that performance of heat sink can be enhanced by increasing the number of channels in the heat sink and the flow rate through the heat sink.

Li et al. [9] presented a detailed numerical study of a forced convection heat transfer occurring in a silicon-based microchannel heat sink using simplified three-dimensional conjugated heat transfer model. Detailed influences of the geometric channel parameters and thermo-physical fluid properties on the heat transfer characteristics were examined. They indicated that the thermophysical properties of the fluid can significantly influence both the flow and heat transfer in a microchannel heat sink. Extending this study, Li and Peterson [10] employed the numerical simulation to optimize the microchannel heat sink geometry under constant pumping power condition. They found that both the physical geometry of the microchannel and the thermo-physical properties of the substrate are important parameters in the design and optimization of the microchannel heat sink. Qu and Mudawar [11,12] investigated the pressure drop and heat transfer in a single-phase microchannel heat sink both numerically and experimentally. In their numerical simulation, the heat transfer characteristics were obtained by solving the conjugate heat transfer problem involving simultaneous determination of the temperature field in both solid and fluid regions. They compared the numerical results with the experimentally measured data and showed good agreement in pressure drop across the microchannel heat sink and local fluid and wall temperature variations.

Experimental and numerical analysis of the effect of axial conduction on the heat transfer in microchannel heat sink with triangular microchannels were performed by Tiselj et al. [13]. They pointed out that the bulk water and heated wall temperatures did not change linearly along the channel. In the study of Lee et al. [14], experiments were conducted to explore the validity of classical correlations based on conventional sized channels for predicting the thermal behavior in single-phase flow through rectangular microchannels. A numerical simulation were also carried out and compared with the experimental data. They pointed out that both fluid flow and heat transfer are in developing regime and cannot be neglected in the analysis.

In the numerical simulations mentioned above, the computation domain consists of only a single channel and the corresponding slice of wall with symmetrical boundary conditions. This kind of computational domain is referred to as the reduced model in the study of Tiselj et al. [13]. As pointed out by Tiselj et al. [13] and Hetsroni et al. [15], complete domain including geometric configurations of the inlet/outlet, microchannel and heat sink base plate should be included in the simulation in order to obtain results that agree with the experimental data. That is, the entire microchannel heat sink should be used as the computation domain instead of a single unit cell.

In practical situations, the fluid supplied to and collected from the microchannel heat sink are via the inlet and outlet. There are many ways to arrange the inlet/outlet locations for the heat sink. The inlet/outlet arrangement is expected to affect the fluid flow and heat transfer characteristics inside the heat sink. Detailed understanding of the inlet/outlet arrangement effect on the heat sink performance is required to enhance the heat sink performance. In this study, fluid flow and heat transfer in microchannel heat sinks with different inlet/outlet arrangements are numerically analyzed

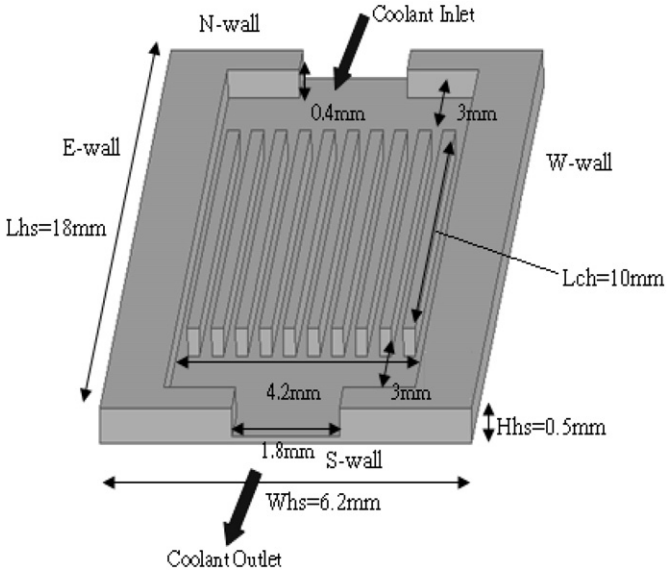

Fig. 1. Geometric configuration of I-type microchannel heat sink.

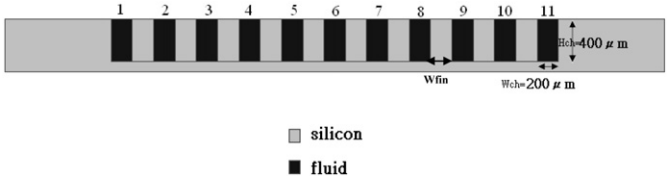

Fig. 2. Heat sink microchannel dimensions.

with computational domain including the entire microchannel heat sink. This work intends to obtain the overall information on the fluid flow and heat transfer when a microchannel heat sink is operated.

2. Microchannel heat sink geometric configurations

The geometric configuration of one of the microchannel heat sinks to be studied is shown in Figs. 1 and 2. The size of microchannel heat sink is fixed with $W_{hs} = 6.2$ mm, $L_{hs} = 18$ mm, and $H_{hs} = 0.5$ mm. The electronic chip that has heat generation is assumed directly attached to the base plate of the heat sink. It is noted that the base area of the microchannel heat sink is about the same as the CPU chip that used in the computer. The microchannel has a rectangular cross section with dimensions of $W_{ch} = 200$ μm, $L_{ch} = 10$ mm, and $H_{ch} = 400$ μm. The wall thickness that separates the channels is set equal to the channel width, i.e., $W_{ch} = W_{fin}$. Because of fixed value of W_{hs}, 11 channels are allowed since enough heat sink edge width is required for bonding a cover plate on the top to form the closed fluid flow passages. As shown in Fig. 1, the width of the heat sink edge is set equal to 1 mm. For the convenience of discussion, the channels are numbered from left to right of the heat sink as indicated in Fig. 2.

At the ends of microchannels, inlet and outlet plenums with width of 4.2 mm and length 3 mm are designed for distributing the fluid flow into and collecting fluid flowing out of the microchannels. The depth of the plenums is the same as that of the channel. By denoting the heat sink sidewalls as E-, W-, N-, and S-walls as shown in Fig. 1, the inlet and outlet can be located at one of the sidewalls that forming the inlet/outlet plenums. They can also be located on the cover plate in the regions near the inlet/outlet plenums. As shown in Fig. 1, the inlet and outlet are located at the centers of N- and S-walls with length of 1.8 mm. Since the overall shape of heat sink with the inlet/outlet arrangement shown in Fig. 1 looks like the letter I, it is therefore referred to as the I-type heat sink in this study.

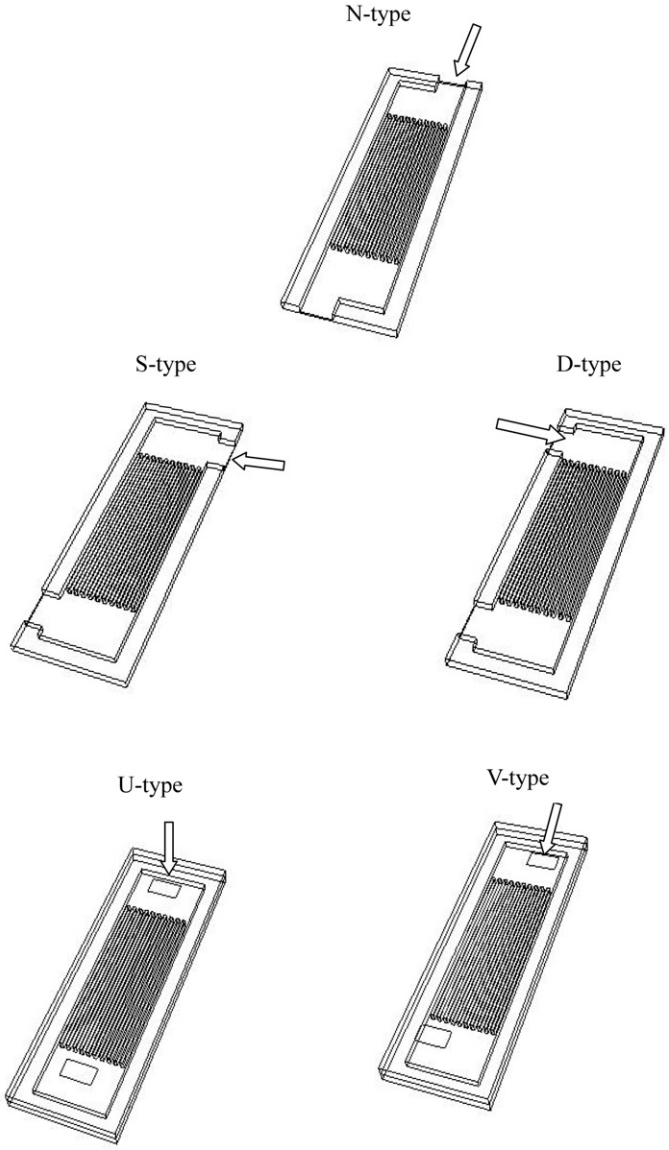

Fig. 3. Geometric configurations of D-, N-, S-, U-, and V-type microchannel heat sinks.

The inlet/outlet arrangement is expected to affect both the fluid flow and heat transfer in the heat sink. In this study, five other types of heat sinks shown in Fig. 3 are designed to investigate the effects of inlet/outlet arrangements on the fluid flow and heat transfer in the heat sinks. In these five types of heat sinks, all the geometric dimensions are the same as those shown in Fig. 1 except for the inlet/outlet locations. The arrows are used to indicate the flow direction at the inlet of the heat sinks. Based on the overall shape of heat sink, they are referred to as N-, D-, S-, U-, and V-type heat sink. In N-type heat sink, inlet and outlet are moved from the centers of the plenum sidewalls to the edges of the heat sink compared with the I-type heat sink. In the D-type heat sink, both the inlet and outlet are located at the center of the E-walls on the inlet/outlet plenums. In the S-type heat sink, the inlet is moved to the W-wall of the inlet plenum compared with the D-type heat sink. In the U-type heat sink, the inlet and outlet open on the top cover plate. The inlet/outlet geometric dimensions with width of 1 mm and length of 1.8 mm are the same as those in Fig. 1 and located right at the central areas of the inlet/outlet plenums. The

V-type heat sink is modified from the U-type heat sink by shifting the inlet/outlet centers with a distance of 0.6 mm toward the W- and E-walls, respectively. With this shifting, the inlet and outlet are located close to the heat sink sidewalls compared with the U-type heat sink. Note that in I-, N-, D-, and S-type heat sinks, fluid flow is supplied and collected horizontally while fluid is supplied and collected vertically in the U- and V-type heat sinks. Using the silicon as material, all the heat sink designs shown in Fig. 3 can be fabricated by etching and anodic bonding techniques. The heat sinks with vertical inlet/outlet design would be easier to implement in the experimental measurement and practical application since they are easier to connect to the fluid supply system.

In this study, we focus on the heat sink inlet/outlet arrangement effect on the fluid flow and heat transfer. The geometric dimensions of the heat sink and channel are fixed. Note that the microchannel number and cross section can be varied by varying the channel width and depth. When the channel width is decreased, number of channels can be increased. However, more computational effort is required since denser grids are needed.

3. Governing equations

To focus on the effect due to the inlet/outlet arrangement on the heat sink performance, the following assumptions are made:

(1) Both fluid flow and heat transfer are in steady-state and three-dimensional.
(2) Fluid is in single phase and flow is laminar.
(3) Properties of both fluid and heat sink material are temperature-independent.
(4) All the surfaces of heat sink exposed to the surroundings are assumed to be insulated except the base plate of heat sink where constant heat flux simulating the heat generation from electronic chip is specified.

Based on above assumptions, the governing equations for fluid and energy transport are

Fluid flow:

$$\nabla \cdot \vec{V} = 0 \tag{1}$$

$$\rho(\vec{V} \cdot \nabla \vec{V}) = -\nabla p + \mu \nabla^2 \vec{V} \tag{2}$$

Energy in fluid flow:

$$\rho c_p(\vec{V} \cdot \nabla T) = k \nabla^2 T \tag{3}$$

Energy in heat sink solid part:

$$k_s \nabla^2 T_s = 0 \tag{4}$$

The boundary conditions for these equations are related to the heat sink operating conditions. In practical applications, heat sink is attached to a heat generation source such as electronic chip to receive heat and dissipate it by fluid flow through the heat sink. The fluid with given temperature and flow rate is supplied by an external pump. The pressure drop across the heat sink can be measured by a pressure transducer connected at the inlet and out of the heat sink. Since pressure drop is related to flow rate, either flow rate or pressure drop can be specified in the numerical simulation. In this study, specifying pressure drop is adopted based on the study of Li et al. [9]. That is, fluid is pumped into the heat sink with a given pressure at the inlet. The inlet pressure must be high enough to overcome the pressure losses when the heat sink is under operation. Based on the operating conditions described above, the boundary conditions for the governing equations are given as,

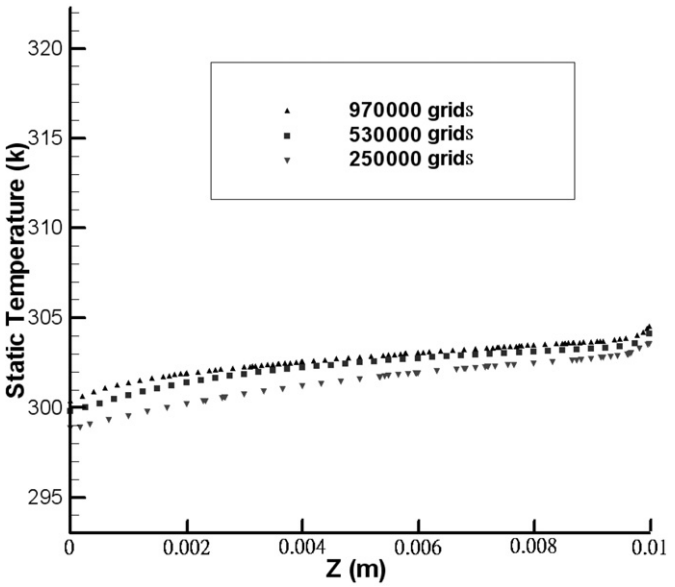

Fig. 4. Comparison of fluid temperature along #11 channel in I-type heat sink using three different grids.

Inlet:

$$p = p_{\text{in}}, \qquad T = T_{\text{in}} \tag{5a}$$

Outlet:

$$p = p_{\text{out}}, \qquad \frac{\partial T}{\partial n} = 0 \tag{5b}$$

Fluid–solid interface:

$$\vec{V} = 0, \qquad T = T_s, \qquad -k_s \frac{\partial T_s}{\partial n} = -k \frac{\partial T}{\partial n} \tag{5c}$$

At the base plate:

$$q_w = -k_s \frac{\partial T_s}{\partial n} \tag{5d}$$

In Eq. (5), p_{in} and T_{in} are the fluid inlet pressure and temperature, respectively, p_{out} is the pressure at the outlet, $n$is the direction normal to the wall or the outlet plane, and q_w is the heat flux applied at the base plate of the heat sink. The pressure drop across the heat sink is defined as $\Delta p = p_{\text{in}} - p_{\text{out}}$.

4. Numerical parameters and procedures

Before the numerical computations, several numerical parameters must be specified in advance. The heat sink material is silicon and the working fluid is deionized water. The inlet water temperature is fixed at 293 K. The pressure drop across the heat sink is chosen in the range of 25 to 50 kPa. The heat flux q_w applied at the heat sink base plate is fixed at 100 W/cm^2. The properties of water and solid used in the computation are $\rho = 1000$ kg/m^3, $c_p = 4182$ J/kg K, $\mu = 0.001$ kg/ms, $k = 0.6$ W/m K, and $k_s = 148$ W/m K.

A general-purpose finite volume based CFD software Fluent v.6.2 is employed to carry out the computation [17]. Computational cells with 2.5×10^5, 53×10^5 and 97×10^5 grids are used to test the grid dependence of the solution. In Fig. 4, the water bulk temperature variations along the #11 channel in the I-type heat sink are shown using the three grid systems under $\Delta p = 50$ kPa. It is seen that almost identical results are predicted when 53×10^5 and 97×10^5 grids are used. Based on the results shown in Fig. 4, a computational cell with 53×10^5 grids as shown in Fig. 5 is employed throughout the computation in this study. The energy

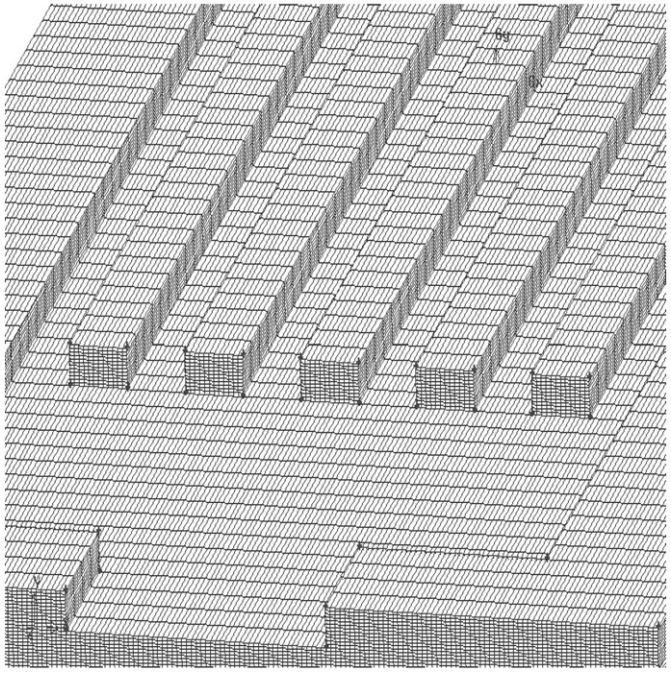

Fig. 5. Computational grids used in the computation.

balance between heat absorbed by water flow Q_{flow} and the total heat rate applied to the heat sink and local Nusselt number variation along the channel $Nu(x)$ can also be used to further ensure the accuracy of the computation. These two quantities can be computed from the following expressions,

$$Q_{\text{flow}} = \dot{m} c_p (T_{\text{out}} - T_{\text{in}}) \tag{6}$$

$$Nu(x) = \frac{h(x) D_h}{k} = \frac{q_w D_h}{k(\bar{T}_w - T_b)} \tag{7}$$

Where $\dot{m}$ is the mass flow rate flowing through the heat sink, $h(x)$ is the local heat transfer coefficient, $\bar{T}_w$ is the local averaged microchannel wall temperature, T_b is the local fluid bulk temperature, and D_h is the hydraulic diameter of the channel defined as

$$D_h = \frac{2 W_{\text{ch}} H_{\text{ch}}}{W_{\text{ch}} + H_{\text{ch}}} \tag{8}$$

In Table 1, the percentage of relative differences between the applied heat rate to the heat sink and heat absorbed by water are shown for six types of heat sinks studied under $\Delta p = 50$ kPa. It is found the maximum relative difference is within 6% indicating that the chosen computation grid produces acceptable results. It is noted that this error is due to the numerical discretization and constant properties assumption for both fluid and solid. Although the error may be further reduced by using finer grid size and taking the temperature-dependent properties for both water and silicon into account, the computation effort increases tremendously. In Fig. 6, the computed Nusselt number along the #5 channel of I-type heat sink is compared with the theoretical correlation given by Phillips [18] with three-side heating correction. It is seen that the computed and theoretical results are in good agreement. The results shown in Fig. 6 indicate that the heat transfer in microchannel takes place in the thermally developing regime. This can be verified through the calculation of the thermal entrance length $x_{\text{fd},t}$ using the following approximation [19]

$$x_{\text{fd},t} = 0.005 D_h Re_{D_h} Pr \tag{9}$$

Where Re_{D_h} is the Reynolds number based on D_h, Pr is the Prandtl number. As will be discussed later, the averaged fluid velocity in this channel is equal to 5 m/sec. The Reynolds number based on the averaged velocity and channel hydraulic diameter is 1333. The computed $x_{\text{fd},t}$ using Eq. (9) is about 74 mm which is greater than the microchannel length of 10 mm employed in this study.

Table 1
Comparison of heat absorbed by fluid and total heat rate applied to heat sinks.

	I	N	D	S	U	V
Q_{flow} (W)	105	107	106	106	107	107
$\left\lvert \frac{Q_{\text{flow}} - q_w W_{\text{hs}} L_{\text{hs}}}{q_w W_{\text{hs}} L_{\text{hs}}} \right\rvert \times 100\%$	5.4	3.6	4.5	4.5	3.6	3.6

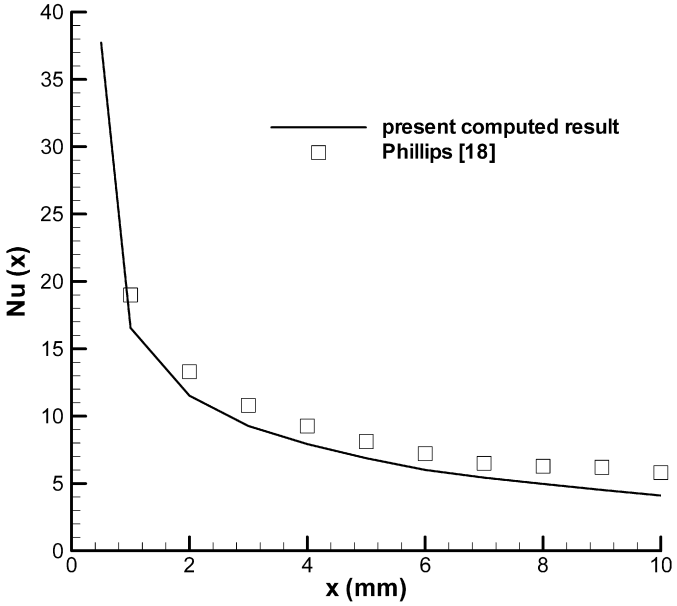

Fig. 6. Comparison of computed and theoretical local Nusselt number variation along the #5 channel in I-type heat sink. $\Delta p = 50$ kPa.

5. Results and discussion

5.1. Flow field

In Fig. 7, the typical overall flow field feature in the six types of heat sinks studied are shown for $\Delta p = 50$ kPa. The velocity vectors taken at the mid-plane of the heat sink are employed to represent the flow fields. As shown in Fig. 7, there exist recirculation zones at the corners of inlet/outlet plenums in the I-, N-, D-, and S-type heat sinks. The size and location of the recirculation zones depend on the inlet/outlet location. In these heat sinks, fluid is supplied to and leaves the heat sinks horizontally from different inlet/outlet locations. Fundamentally, the flow fields in these heat sinks are similar to the cavity flow having different inlet/outlet locations without microchannels [20,21]. In such flow field, existence of recirculation zones at the corners of cavity is expected. In the U- and V-type heat sink, the fluid is supplied and leaves the heat sink vertically. At the inlet plenum, it looks more like a jet impinging on the bottom wall of the inlet plenum. Because of the small vertical dimension of plenum, no recirculation zone appeared in the inlet/outlet plenums for these two types of heat sinks.

The flow pattern at the inlet plenum certainly affects the fluid velocity at the entrance of the microchannels. This referred to as the velocity maldistribution [22,23]. To address this point, we compute the averaged velocity in each channel of the heat sinks and the results are shown in Fig. 8. In Fig. 8, averaged velocities in each channel are shown for various pressure drops. The velocity magnitude decreases with the decrease in pressure drop but the

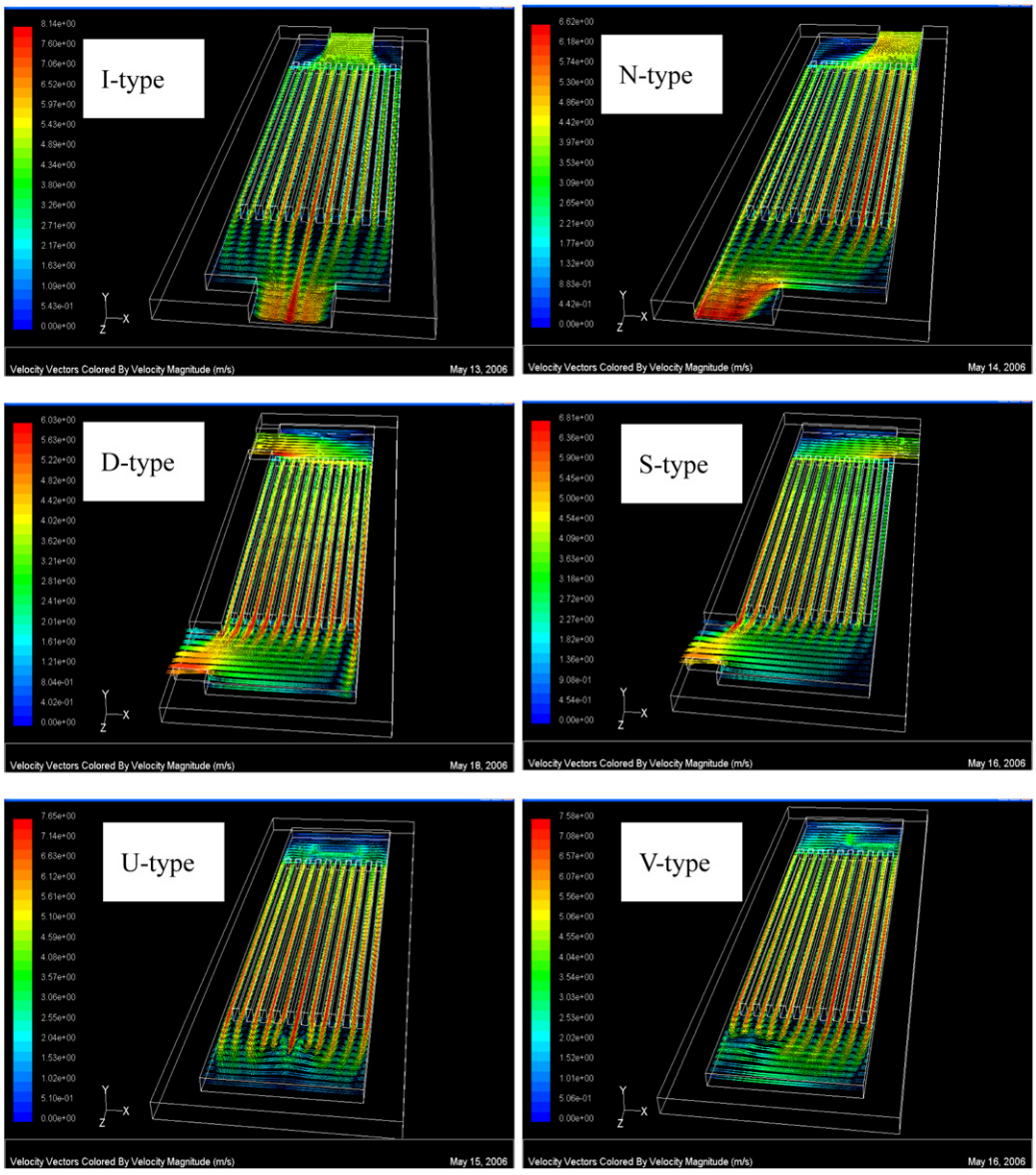

Fig. 7. Flow fields of microchannel heat sinks represented by velocity vectors at the mid-plane of heat sinks. $\Delta p = 50$ kPa.

variation trends are the same in each type of heat sink. This is because small pressure drop corresponds to small flow rate driven into the heat sink. Because of the difference of the flow patterns in the inlet plenums, averaged velocity in each channel is different under a given pressure drop. For I- and N-type heat sinks, the channels located right opposite to the inlet would have higher averaged velocities as expected. The averaged velocities for other channels are seen to decrease depending on their distances from the inlet. Because of symmetry, the velocity distribution for I-type heat sink is symmetrical with respect to the centerline of the heat sink. For D-type heat sink, the lowest and highest averaged velocities occur in #1 and #3 channels, respectively. The velocities in other channels have a fairly constant value. In the S-type heat sink, it is interesting to point out that the highest averaged velocity occurs at #1 channel instead of #9 channel as would be predicted in the D-type heat sink. The reason for this observation is because the outlet produces a suction effect that results in increasing velocity in #1 channel. It is also seen that #11 channel in S-type heat sink has the lowest averaged velocity among the six types of heat sinks studied under a given pressure drop. In the U-type heat sink, the incoming fluid flow impinges on the bottom wall and spreads out all around the inlet plenum. Due to the flow is confined by the plenum sidewalls, flow hitting on the sidewalls will bounce back and re-direct into the channels. As a result, higher fluid flow velocities can be found in the channels near the inlet portion (#6 channel) and near the sidewalls (#1 and #11 channels). The lowest fluid velocities occur at #3 and #9 channels since they receive less rebounded flow from sidewalls and inlet portion as compared to other channels. Due to geometric symmetry, averaged velocity distribution in U-type heat sink is symmetrical with respect to the centerline of the heat sink. In V-type heat sink, the jet impingement is moved to a location near the edge of heat sink, higher fluid velocities can be found for channels located near the inlet portion (#8, #9, and #10 channels) and in the region near the edge of heat sink (#1 channel). The lowest fluid velocity occurs at #5 channel since its location has longest distance from the inlet and sidewall. Based on the results shown in Fig. 8, it is seen that better flow velocity uniformity can be obtained in the U- and V-type heat sinks. The flow uniformity directly affects the temperature distribution of the entire

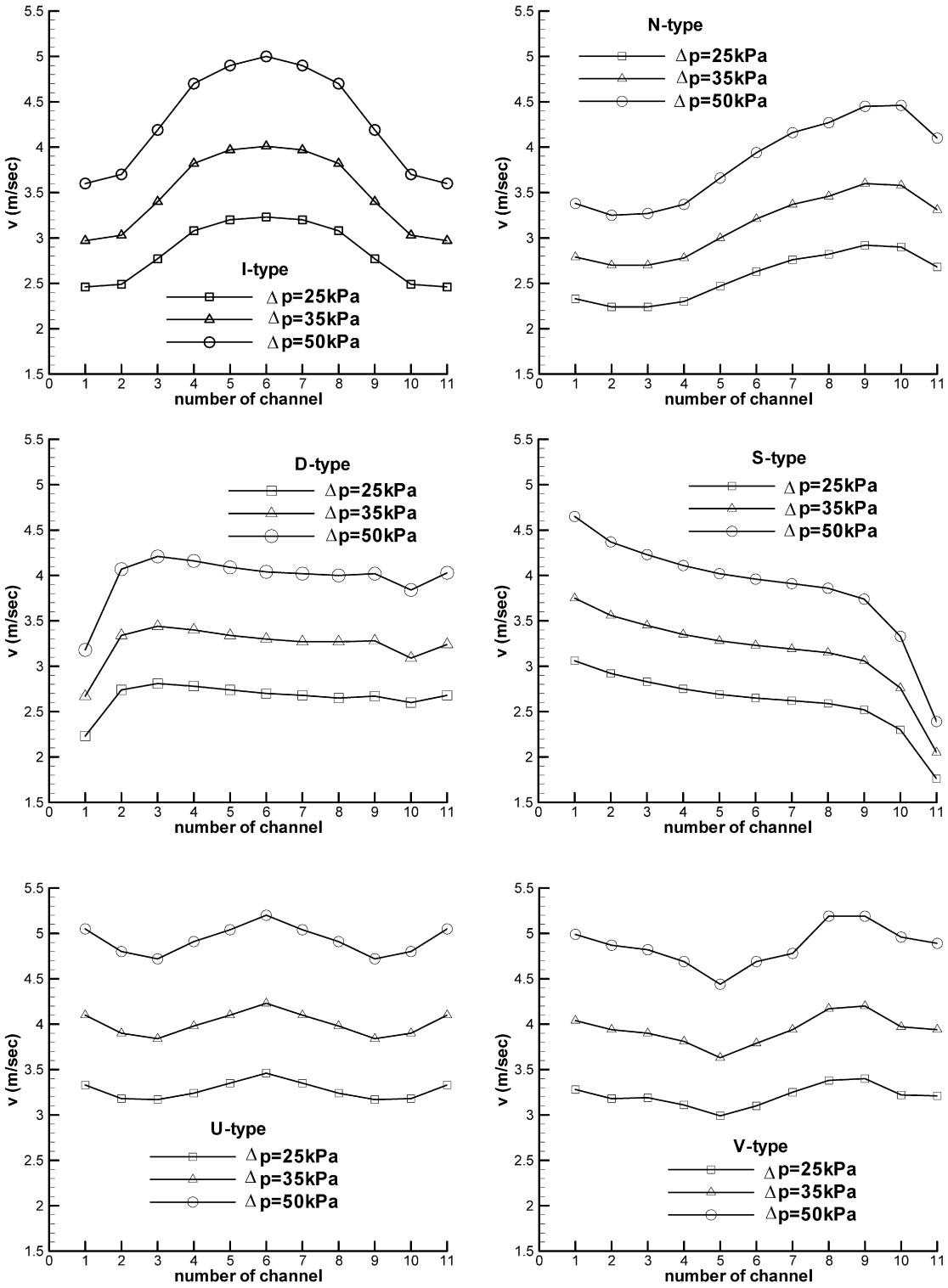

Fig. 8. Averaged velocity in each channel of microchannel heat sinks as function of pressure drops.

heat sink and consequently the heat sink performance which will be discussed below.

From Fig. 8, it is seen that the velocity is in the range of 2 to 5 m/sec for the chosen pressure range. The corresponding Reynolds number is from 530 to 1330 based on channel hydraulic diameter. This validates the assumption of laminar flow in the heat sink. For higher pressure drops, the laminar flow assumption may become invalid due to the increase in Reynolds number.

5.2. Temperature distributions

The temperature distributions of the solid part of the heat sinks corresponding to Fig. 7 are presented in Fig. 9. For all six types of heat sink studied, it is found that the high temperature region occurs at the edge of the heat sinks since there is no heat dissipation by fluid convection. The low-temperature region occurs in the region where microchannels are placed, especially at the en-

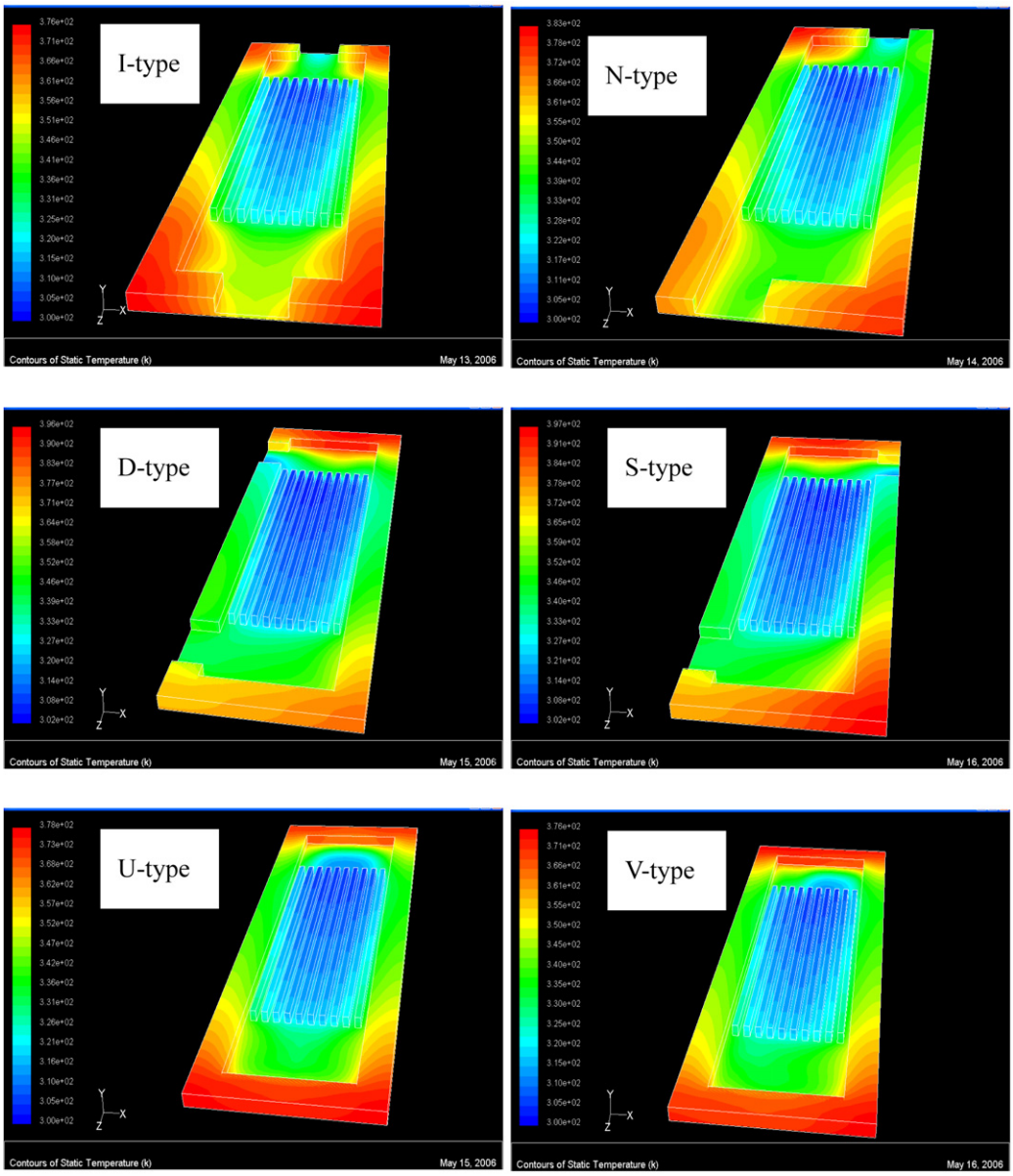

Fig. 9. Temperature distribution of the solid part of microchannel heat sinks. $\Delta p = 50$ kPa.

trance regions of the channels. The reason for this result is clearly due to the high heat transfer coefficient in the entrance zone of the microchannels. It is known that both hydrodynamic and thermal entry lengths depend on the fluid flow Reynolds number. In Fig. 8, we have demonstrated the maldistribution of fluid velocities in each channel due to the different inlet/outlet arrangement, it is then expected that both the hydrodynamic and thermal entry lengths would be different in each channel. As a result, the non-uniform temperature distribution in the heat sink is expected and depends on the inlet/outlet locations.

In the heat sink operation, coolant flow is used to dissipate heat away by convection. It is therefore also necessary to understand the fluid temperature variations subject to the effect of inlet/outlet arrangement. To address this point, the averaged fluid temperatures in each channel are shown in Fig. 10. It is clearly seen that when fluid velocity in channel is low, higher averaged fluid temperature is resulted. The simple theory regarding the heat transfer characteristics in a channel subject to constant heat flux can be used to explain this observation. As the fluid velocity in channel is low, fluid temperature would be increase in order to carry specified heat flux away. It is also noted that all the temperature profiles shown in Fig. 10 indicates that the lower averaged temperatures occur in the channels located near the center of the heat sink. For fluids in channels close to the edge of heat sink, higher fluid temperatures are observed due to the heat transfer from the high-temperature edge of the heat sink.

In the experimental study, the temperature at the base plate of heat sink is usually measured to quantify the performance of the heat sink. It is usually difficult to measure the base plate temperature distribution since it is bonded with the chip surface or the heat spreader. By taking the advantage of numerical simulation, temperature distribution on the heat sink base plate can be easily obtained. In Fig. 11, the temperatures on the base plates of six types of heat sink studied are presented to realize their distributions. For all six heat sinks, it is found that the maximum temperature which used to quantify the thermal resistance of heat sink always occurs at the corners of the heat sinks while minimum temperature occurs in the region near the microchannel entrance

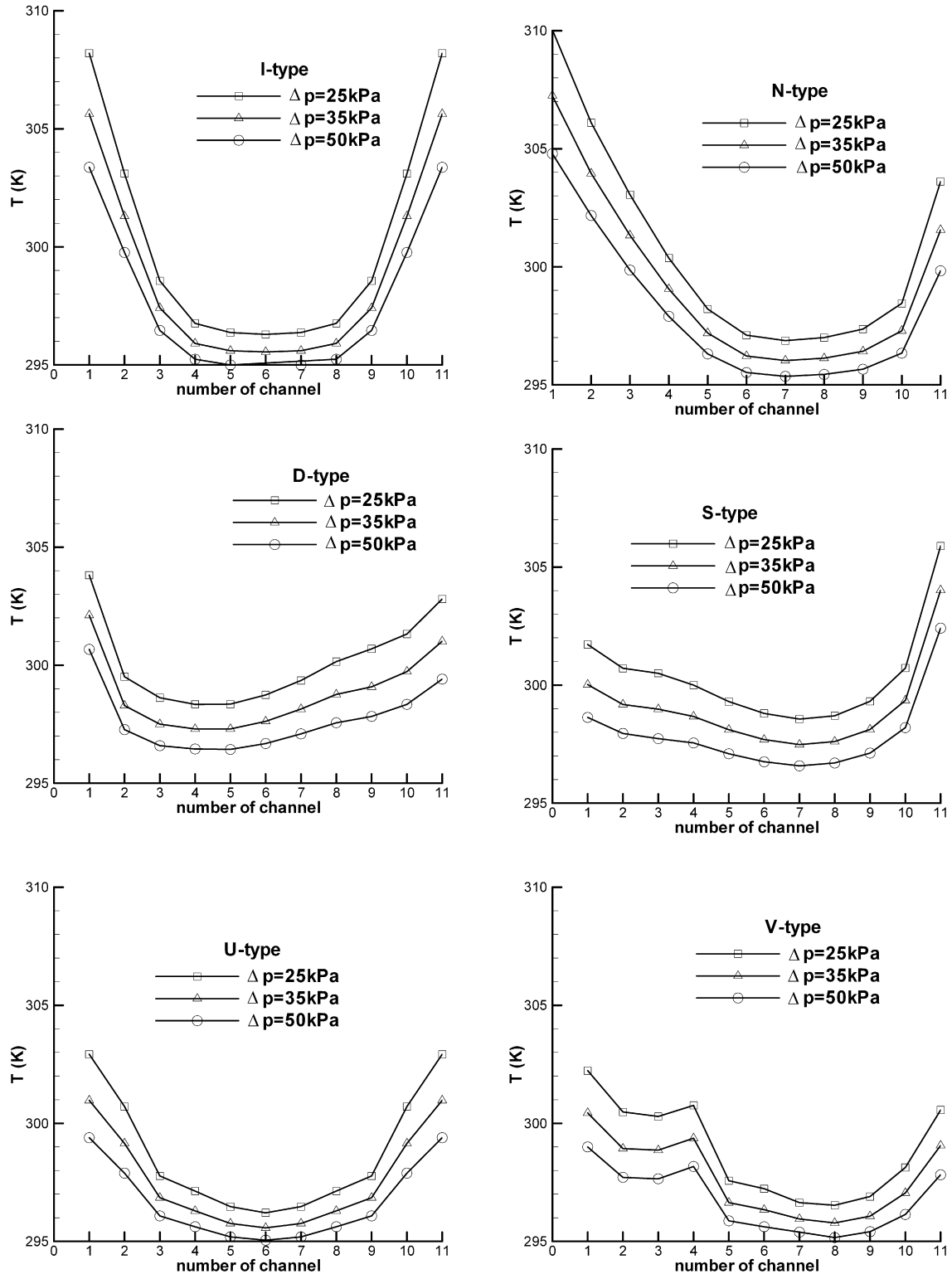

Fig. 10. Averaged fluid temperature in each channel of microchannel heat sinks as function of pressure drops.

zones. Based on the results shown in Figs. 10 and 11, it is seen that U-, V-type heat sinks have better surface temperature uniformity as compared to I-, N-, S-, and D-type heat sinks.

5.3. Overall heat sink thermal resistance

In this study, the overall heat sink performance is determined by three parameters, the thermal resistance, overall heat transfer coefficient and pressure drop coefficient. The heat sink thermal resistance is defined as,

$$R_{\mathrm{th}} = \frac{T_{w\max} - T_{\mathrm{in}}}{q_w W_{\mathrm{hs}} L_{\mathrm{hs}}} \tag{10}$$

Where $T_{w\max}$ is maximum temperature of the heat sink base plate. Using this definition, R_{th} for each type of heat sink as a function of pressure drop is computed and shown in Fig. 12. It is

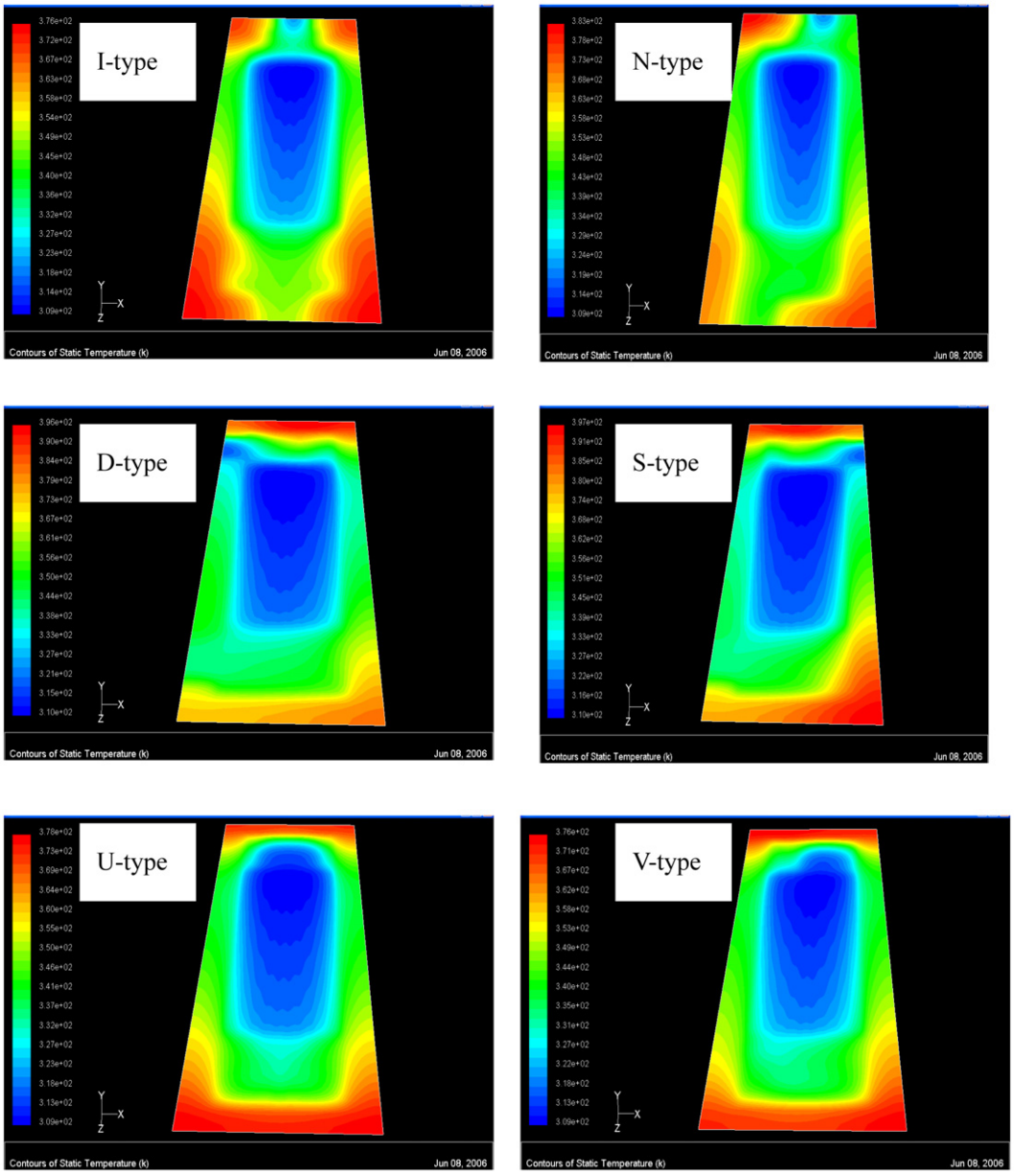

Fig. 11. Temperature distributions of the base plates of microchannel heat sink. $\Delta p = 50$ kPa.

found that the heat sink thermal resistance decreases with the increase in pressure drop. Since the flow rate is proportional to the pressure drop increase, it implies that lower heat sink thermal resistance can be achieved under higher pressure drop and flow rate. However, the bonding strength of the cover plate usually sets the limit for the pressure drop. Based on results shown in Fig. 12, it is seen that the V-type heat sink has the best performance while S-type has the worst performance among the heat sinks studied.

The heat sink overall heat transfer coefficient is defined as,

$$\overline{Nu} = \bar{h} D_h / k \tag{11}$$

$$\bar{h} = q_W / (T_{\mathrm{hs,ave}} - T_{\mathrm{ave}}) \tag{12}$$

where $T_{\mathrm{hs,ave}}$ and T_{ave} are the overall averaged temperatures of both heat sink and coolant, respectively. $T_{\mathrm{hs,ave}}$ is computed by summing temperatures at solid grids and divided by the total solid grid number. It may be thought as the volume averaged temperature of the solid part of the heat sink. T_{ave} is computed in similar way as that of $T_{\mathrm{hs,ave}}$. As shown in Fig. 13, the V-type heat sink has highest heat transfer coefficient which is in consistent with the results shown in Fig. 12 for the thermal resistance.

In heat sink operation, pressure drop across the heat sink is one of important factors that determine heat sink performance. The coolant pressure at the heat sink inlet must be high enough to overcome all the pressure losses occurred inside the heat sink which can be expressed as,

$$\Delta p = \Delta p_{\mathrm{in},1} + \Delta p_{\mathrm{in},2} + \Delta p_{\mathrm{ch}} + \Delta p_{\mathrm{ex},1} + \Delta p_{\mathrm{ex},2} \tag{13}$$

where $\Delta p_{\mathrm{in},1}$, $\Delta p_{\mathrm{in},2}$, Δp_{ch}, $\Delta p_{\mathrm{ex},1}$ and $\Delta p_{\mathrm{ex},2}$ are the pressure drops from inlet port to inlet plenum due to flow sudden expansion, from inlet plenum to channel inlets due to flow contraction, from channel inlet to exit due to wall friction, from channel exits to outlet plenum due to flow sudden expansion and from outlet plenum to outlet port due to flow contraction, respectively. In this study, we specify the pressure drop across the heat sink and flow rate through the heat sink was computed. Similar to Darcy–Weisbach equation, pressure drop and flow rate can be related as,

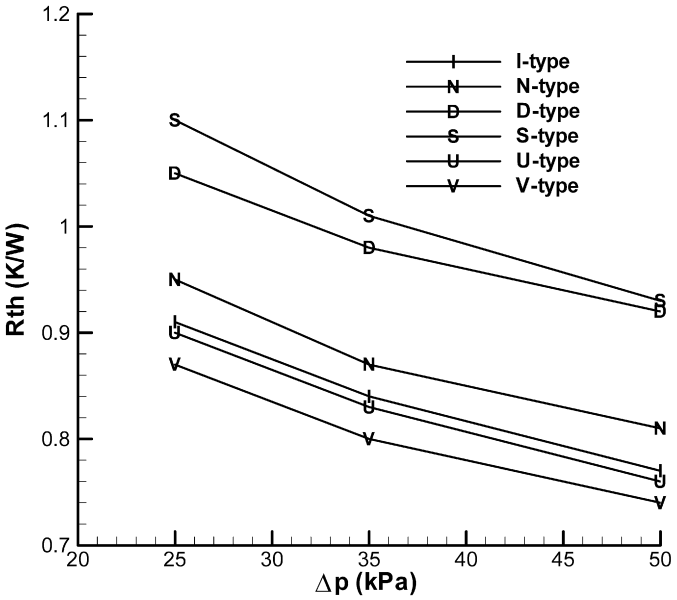

Fig. 12. Thermal resistance of microchannel heat sink as a function of pressure drop.

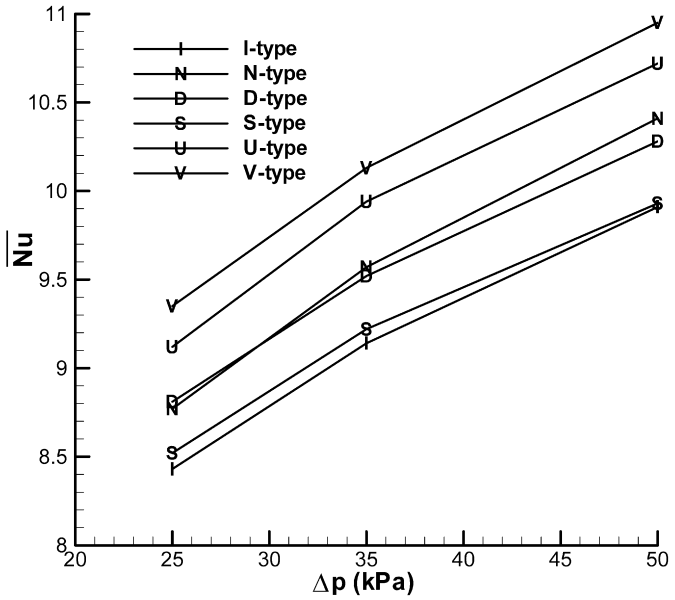

Fig. 13. Overall heat transfer coefficients of microchannel heat sink as a function of pressure drop.

Table 2
Relations between pressure drop, flow rate and pressure drop coefficient in the heat sink operation.

Type of heat sink		I	N	D	S	U	V
Q	$\Delta p = 50$ kPa	3.2×10^{-6}	2.9×10^{-6}	3×10^{-6}	2.9×10^{-6}	3.8×10^{-6}	3.7×10^{-6}
(m^3/s)	$\Delta p = 35$ kPa	2.6×10^{-6}	2.3×10^{-6}	2.4×10^{-6}	2.3×10^{-6}	2.9×10^{-6}	2.9×10^{-6}
	$\Delta p = 25$ kPa	2.1×10^{-6}	1.9×10^{-6}	2×10^{-6}	1.9×10^{-6}	2.4×10^{-6}	2.4×10^{-6}
F	$\Delta P = 50$ kPa	10×10^{12}	13×10^{12}	12×10^{12}	13×10^{12}	8×10^{12}	8×10^{12}
(m^{-4})	$\Delta P = 35$ kPa	10×10^{12}	13×10^{12}	12×10^{12}	13×10^{12}	8×10^{12}	8×10^{12}
	$\Delta P = 25$ kPa	10×10^{12}	13×10^{12}	12×10^{12}	13×10^{12}	8×10^{12}	8×10^{12}

$$\Delta p = \frac{1}{2}\rho F Q^2 \tag{14}$$

Where F is defined as the pressure drop coefficient and Q is the fluid flow rate flowing through the heat sink. Computed pressure drop, flow rate and pressure drop coefficient results for each type of heat sink are summarized in Table 2. Note that the pressure drop coefficient for a given heat sink geometry has a fixed value as indicated in Table 2. In I-, D, N- and S-type heat sinks, the fluid flow is supplied and corrected horizontally. There is no change in flow direction before it is distributed into and corrected from the channels. The flow recirculations appeared in the inlet/outlet plenums characterize the fluid velocity at the channel inlets and exits. In the U- and V-type heat sinks, the flow from the inlet impinges on the bottom wall of heat sink and redistributes to the microchannels. At the outlet, fluid changes direction and flows out of the heat sink vertically. Although changing flow direction causes more pressure drop as in the U- and V-type heat sinks, the velocity distributions in U- and V-type heat sinks are more uniform as compared with those of I-, N-, D-, and S-type heat sinks. As a result, less $\Delta p_{in,2}$ and $\Delta p_{ex,1}$ are expected in the U- and V-type heat sinks. Consequently, smaller pressure drop coefficients for U- and V-type heat sinks are found as indicated in Table 2. This implies that higher flow rate and lower thermal resistance can be achieved in the U- and V-types of heat sink.

6. Conclusion

Numerical simulations on the fluid flow and heat transfer in full scale microchannel heat sinks were performed in this study. According to the inlet/outlet arrangements, performances of six types of heat sink were studied. Under the same geometric dimensions among these six types of heat sinks except the inlet/outlet locations, the following conclusions can be made based on the simulated results:

(1) For all the heat sinks studied, it is found that the highest heat sink temperature takes place at the edge of the heat sink since there is no heat dissipation by fluid convection.
(2) The low-temperature region of heat sink occurs at the entrance zones of the microchannels due to high heat transfer coefficient. Heat sink temperature increases along the flow direction because of constant heat flux applied at the heat sink base plate.
(3) For the heat sinks with horizontally fluid supply and collection, i.e., the I-, N-, D-, and S-type heat sinks, the velocity maldistribution is more serious than heat sinks with vertically fluid supply and collection, i.e., the U- and V-type heat sinks.
(4) Because of velocity maldistribution, the flow rate in each heat sink channel is different. As a result, temperature nonuniformity is more serious in the heat sinks with horizontally fluid supply and collection.
(5) Using the thermal resistance, overall heat transfer coefficient and pressure drop coefficient to evaluate the heat sink performance, it is found that the V-type heat sink has the best performance among the heat sinks studied.

References

[1] S.G. Kandlikar, W.J. Grande, Evolution of microchannel flow passages – thermohydraulic performance and fabrication technology, Heat Transfer Engineering 24 (2003) 3–17.
[2] D.B. Tuckerman, R.F. Pease, High-performance heat sinking for VLSI, IEEE Electronic Devices Letters, EDL-2 (1981) 126–129.

[3] R.W. Knight, D.J. Hall, J.S. Goodling, R.C. Jaeger, Heat sink optimization with application to microchannels, IEEE Transactions on Components, Hybrids, and Manufacturing Technology 15 (1992) 832–842.
[4] H.Y. Zhang, D. Pinjala, T.N. Wong, Y.K. Joshi, Development of liquid cooling technologies for flip chip ball grid array packages with high heat flux dissipations, IEEE Trans. Components Packag. Technol. 28 (2005) 127–135.
[5] C.Y. Zhao, T.J. Lu, Analysis of microchannel heat sinks for electronics cooling, Intl. J. Heat Mass Transfer 45 (2002) 4857–4869.
[6] S.J. Kim, D. Kim, Forced convection in microstructures for electronic equipment cooling, ASME J. Heat Transfer 121 (1999) 639–645.
[7] A.G. Fedorov, R. Viskanta, Three-dimensional conjugate heat transfer in the microchannel heat sink for electronic packaging, Int. J. Heat Mass Transfer 43 (2000) 399–415.
[8] K.K. Ambatipudi, M.M. Rahman, Analysis of conjugate heat transfer in microchannel heat sinks, Numerical Heat Transfer Part A 37 (2000) 711–731.
[9] J. Li, G.P. Peterson, P. Cheng, Three-dimensional analysis of heat transfer in a micro-heat sink with single phase flow, Int. J. Heat Mass Transfer 47 (2004) 4215–4231.
[10] J. Li, G.P. Peterson, Geometric optimization of a micro heat sink with liquid flow, IEEE Trans. on Component Pack. Tech. 29 (2006) 145–154.
[11] W. Qu, I. Mudawar, Analysis of three-dimensional heat transfer in microchannel heat sinks, Int. J. Heat Mass Transfer 45 (2002) 3973–3985.
[12] W. Qu, I. Mudawar, Experimental and numerical study of pressure drop and heat transfer in a single-phase micro-channel heat sink, Int. J. Heat Mass Transfer 45 (2002) 2549–2565.
[13] I. Tiselj, G. Hetsroni, B. Mavko, A. Mosyak, E. Pogrebnyak, Z. Segal, Effect of axial conduction on the heat transfer in microchannels, Int. J. Heat Mass Transfer 47 (2004) 2551–2565.
[14] P. Lee, S.V. Garimella, D. Liu, Investigation of heat transfer in rectangular microchannels, Int. J. Heat Mass Transfer 48 (2005) 1688–1704.
[15] G. Hetsroni, A. Mosyak, Z. Segal, Nonuniform temperature distribution in electronic devices cooled by flow in parallel micro-channels, IEEE Trans. Components Packag. Technol. 24 (2001) 16–23.
[16] T.M. Harms, M.J. Kazmierczak, F.M. Cerner, Developing convective heat transfer in deep rectangular microchannels, Int. J. Heat Fluid Flow 20 (1999) 149–157.
[17] Fluent 6 User's Guide, Lebanon, NH, Fluent Inc., 2000.
[18] R.J. Phillips, Microchannel heat sinks, PhD thesis, Massachusetts Institute of Technology, 1987.
[19] F.P. Incropera, D.P. DeWitt, Fundamentals of Heat and Mass Transfer, John Wiley and Sons, New York, 1996.
[20] X. Shi, J.M. Khodadadi, Fluid flow and heat transfer in a lid-driven cavity due to an oscillating thin fin: transient behavior, ASME J. Heat Transfer 126 (2004) 924–930.
[21] P.N. Shankar, M.D. Deshpande, Fluid mechanics in the driven cavity, Annu. Rev. Fluid Mech. 32 (2000) 93–136.
[22] M. Lu, C. Wang, Effect of the inlet location on the performance of parallel-channel cold-plate, IEEE Trans. Components Packag. Technol. 29 (20016 30–38.
[23] J.T. Tseng, J.C. Chu, M.S. Lu, C.C. Wang, R. Grief, Investigation of the flow maldistribution in microchannels, in: ASME Congress 2003, IMECE2003-41, p. 323.